

Incorporating NASA Spaceborne Radar Data into NOAA National Mosaic QPE System for Improved Precipitation Measurement: A Physically Based VPR Identification and Enhancement Method

YIXIN WEN,* QING CAO,⁺ PIERRE-EMMANUEL KIRSTETTER,[#] YANG HONG,[@] JONATHAN J. GOURLEY,[&]
JIAN ZHANG,[&] GUIFU ZHANG,^{**} AND BIN YONG⁺⁺

^{*} School of Meteorology, and Advanced Radar Research Center, University of Oklahoma, and Hydrometeorology and Remote Sensing Laboratory, National Weather Center, Norman, Oklahoma

⁺ Advanced Radar Research Center, University of Oklahoma, and Hydrometeorology and Remote Sensing Laboratory, National Weather Center, Norman, Oklahoma

[#] Advanced Radar Research Center, University of Oklahoma, and Hydrometeorology and Remote Sensing Laboratory, National Weather Center, and NOAA/National Severe Storms Laboratory, Norman, Oklahoma

[@] Advanced Radar Research Center, and School of Civil Engineering and Environmental Sciences, University of Oklahoma, and Hydrometeorology and Remote Sensing Laboratory, National Weather Center, Norman, Oklahoma
& NOAA/National Severe Storms Laboratory, Norman, Oklahoma

^{**} School of Meteorology, University of Oklahoma, Norman, Oklahoma

⁺⁺ Advanced Radar Research Center, University of Oklahoma, and Hydrometeorology and Remote Sensing Laboratory, National Weather Center, Norman, Oklahoma, and State Key Laboratory of Hydrology–Water Resources and Hydraulic Engineering, Hohai University, Nanjing, China

(Manuscript received 16 July 2012, in final form 7 January 2013)

ABSTRACT

This study proposes an approach that identifies and corrects for the vertical profile of reflectivity (VPR) by using Tropical Rainfall Measuring Mission (TRMM) precipitation radar (PR) measurements in the region of Arizona and southern California, where the ground-based Next Generation Weather Radar (NEXRAD) finds difficulties in making reliable estimations of surface precipitation amounts because of complex terrain and limited radar coverage. A VPR identification and enhancement (VPR-IE) method based on the modeling of the vertical variations of the equivalent reflectivity factor using a physically based parameterization is employed to obtain a representative VPR at S band from the TRMM PR measurement at Ku band. Then the representative VPR is convolved with ground radar beam sampling properties to compute apparent VPRs for enhancing NEXRAD quantitative precipitation estimation (QPE). The VPR-IE methodology is evaluated with several stratiform precipitation events during the cold season and is compared to two other statistically based correction methods, that is, the TRMM PR–based rainfall calibration and a range ring–based adjustment scheme. The results show that the VPR-IE has the best overall performance and provides much more accurate surface rainfall estimates than the original ground-based radar QPE. The potential of the VPR-IE method could be further exploited and better utilized when the Global Precipitation Measurement Mission’s dual-frequency PR is launched in 2014, with anticipated accuracy improvements and expanded latitude coverage.

1. Introduction

Studies of various physical processes related to water cycle, which are of interest to the scientific communities of meteorology, hydrology, environment, ecology, agriculture, etc., often require reliable quantitative

precipitation estimation (QPE). Therefore, accurate measurement of precipitation at a range of spatial and temporal resolutions is invaluable for a variety of scientific applications. Weather radar has proven its value to the nation since the installation of the current Weather Surveillance Radar-1988 Doppler (WSR-88D) Next Generation Weather Radar (NEXRAD) network. Based on data measured by the NEXRAD network, the National Mosaic and the next-generation quantitative precipitation estimation system (NMQ/Q2) (Vasiloff et al. 2007; Zhang et al. 2011) is a real-time test bed comprising high-resolution (1 km, 5 min) multisensor

Corresponding author address: Yang Hong, School of Civil Engineering and Environmental Sciences, University of Oklahoma, Atmospheric Radar Research Center at the National Weather Center, 120 David L. Boren Blvd., Norman, OK 73072.
E-mail: yanghong@ou.edu

precipitation products. A web-based display and a rain gauge-based validation system have been built for the datasets and are freely accessible on the Internet. However, because of the lack of adequate ground radar (GR) coverage from intervening terrain blockages (Maddox et al. 2002), reliable ground-based precipitation measurements are difficult to obtain in mountainous regions.

For ground-based volume-scanning weather radars, an important error source that can lead to significant systematic error in radar rainfall estimates is attributed to inaccurate calibration of the radar (Smith et al. 1996). Another major error source, particularly in complex terrain, comes from the lack of representativeness of reflectivity sampled aloft to surface precipitation. Reflectivity varies with height because of the processes of melting, aggregation, collision, coalescence, evaporation, and drop breakup. This problem is exacerbated in complex terrain where ground radars must rely on scans at higher-elevation angles to observe precipitating systems, in which radar observations within the ice region above the melting level are used for QPE. Furthermore, the radar beam broadens with range and could be too wide to accurately resolve the vertical structure of precipitation.

To mitigate radar QPE errors associated with non-uniform vertical profiles of reflectivity (VPRs), a variety of studies have investigated different approaches to derive representative VPRs for improving QPE. The representative VPRs in previous studies include 1) climatological VPR (Joss and Lee 1995, Cao et al. 2013a), 2) retrieved VPR from radar observations at different distances and different altitudes (Koistinen 1991; Joss and Lee 1995; Germann and Joss 2002; Andrieu and Creutin 1995; Vignal et al. 1999, 2000; Vignal and Krajewski 2001, Zhang and Qi 2010), and 3) parameterized VPR (Kitchen et al. 1994; Fabry and Zawadzki 1995; Kitchen 1997; Smyth and Illingworth 1998; Matrosov et al. 2007; Tabary 2007). All of these approaches rely on radar data or other surface observations to obtain the VPRs. However, in mountainous regions (e.g., the analysis region of this study), radar measurements near the surface are less ubiquitous, and the complete VPRs might not be fully obtained. Some observational limitations of ground-based radar can be mitigated by spaceborne radar, whose measurements are much less impacted by mountain blockages, and beam broadening effects in the vertical direction (Iguchi et al. 2000). The spaceborne precipitation radar (PR) onboard the National Aeronautics and Space Administration's (NASA) Tropical Rainfall Measuring Mission (TRMM) satellite, launched in late 1997, is the first weather radar to estimate rainfall over the tropics and subtropics from space (Simpson et al. 1996). The PR operates at Ku band with a frequency of

13.8 GHz (2.17-cm wavelength) and scans across a 215-km-wide footprint, with vertical and horizontal resolutions of 250 m and 4.3 km, respectively, at nadir. Considering that precipitating systems typically extend several kilometers in the vertical direction, the PR's vertical resolution of 250 m ensures fine observations suitable for studying the vertical structures of storms. Although the precipitation attenuates Ku-band PR observations more than S-band ground radar observations, the PR's signal processing algorithms developed by the PR science team (Iguchi et al. 2000, 2009) have shown good performance in correcting for attenuation losses in precipitation (Yong et al. 2010; Wen et al. 2011). Gabella et al. (2006) have used the so-called near-surface reflectivity, which is measured at the lowest pulse volume of PR, to mitigate the ground radar's range-dependent bias on the island of Cyprus.

This study proposes an approach that identifies and corrects for ground-based radar VPRs (NMQ data) by using spaceborne TRMM PR measurements [hereinafter VPR identification and enhancement (VPR-IE)]. The remainder of this paper is organized as follows. The study area and dataset used for correction are described in section 2. A detailed description of the VPR-IE method is provided in section 3. Two other correction methods are discussed in section 4. Section 5 presents case study results for five events representing various meteorological processes in the study area. A summary and discussion of future directions follows in the last section.

2. Study area and dataset

In the current study, we have chosen the region of Arizona and southern California (latitude is from 32° to 37°N, longitude is from -115° to -110°W) as the study area (Fig. 1). QPE in this region is challenging because of the sparseness of rain gauge networks, high spatial variability of precipitation due to orographic enhancements, relatively shallow precipitating clouds, and insufficient NEXRAD radar coverage. The digital elevation map in Fig. 1 shows the topography in this study area, which consists of six smaller regions: the plateau region, the central region, the northwest region, the southwest region, the southeast region, and the northeast region (Sellers and Hill 1974; Watson et al. 1994). The average altitude of the study area is about 1106 m, while the lowest elevation is only 3 m and the highest elevation is 3657 m. The climatological statistics in this area indicate two peaks of precipitation each year: one in the winter caused by large-scale synoptic systems, and the other one in the summer caused by the North American monsoon.

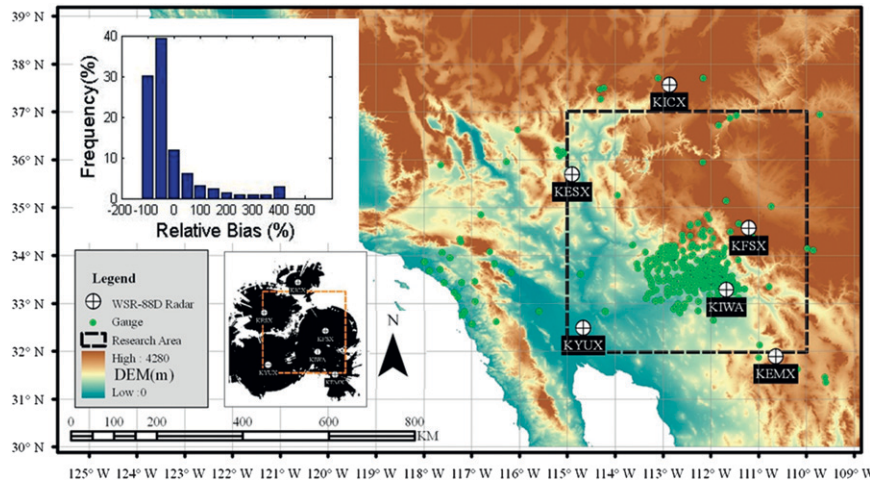


FIG. 1. An image showing the topography around the study area (black dashed box) and the locations of rain gauges (circles) and WSR-88D radar sites (white circles with cross). The inset black and white map shows the radar coverage at 3 km above ground level. The histogram shows the distribution of hourly bias ratio [calculated from $(GR - \text{gauge})/\text{gauge} \times 100\%$] for 3 months of data from 1 Dec 2009 to 28 Feb 2010.

Nearly half of the area has average rainfall of less than 250 mm yr^{-1} . The southwest region receives rainfall amounts of less than 125 mm yr^{-1} . The northern plateau regions have an average rainfall of more than 500 mm yr^{-1} (Sellers and Hill 1974). Experience with more than 3 years of radar data in the NMQ system indicates that the ground radar QPE has significant underestimation issues due to the poor sampling of precipitation. Figure 1 shows that some regions are as far as 100 km or even 200 km from the nearest radar (e.g., 35°N and 113°W at more than 200 km from the nearest radar). The distribution of hourly bias ratios $[(GR - \text{gauge})/\text{gauge} \times 100\%]$ from 1 December 2009 to 28 February 2010 indicates the severe underestimation of precipitation for ground radars. For the six WSR-88D radars included in this study, the surrounding highlands cause partial or even complete beam blockage to radars (especially at lower-elevation angles). At significant distances from the radar (e.g., more than 100 km) this hampers the sampling of precipitation close to the ground with the lower elevation angles. The radar beam might be too high and sample the ice region above the melting layer while it is raining at the surface, causing large errors in surface rainfall estimation because of the vertical variations of reflectivity. In such conditions the radar beam may be too wide to accurately resolve the vertical structure of precipitation. This is particularly true in the case of strong vertical reflectivity gradients, for example, linked to the bright band (Kirstetter et al. 2010). Figure 2c illustrates the effect of beam widening on the apparent ground radar VPRs, which degrades with range. It is clearly shown that the bright band

becomes thicker and less intense with increasing range. The apparent VPR is defined as the VPR influenced by beam broadening. It is noted that because of the earth's curvature and the increase of beam altitude, the radar beam samples less often the lowest part of the VPR with increasing distance. This effect is aggravated by beam blockage due to surrounding highlands.

The NMQ system (Zhang et al. 2011) combines information from ground-based radars comprising the National Weather Service's NEXRAD network. Based on the significant research already performed on the ground-based NMQ data in regards to data quality (Lakshmanan et al. 2007), data mosaicking techniques (Zhang et al. 2005), and rainfall estimation (Vasiloff et al. 2007), the system has been generating high-resolution national 3D reflectivity mosaic grids (31 levels) and a suite of severe weather and QPE products at a 1-km horizontal resolution and 5-min update cycle since June 2006. We have identified five TRMM PR overpasses that meet the following criteria: 1) the maximum time discrepancy between TRMM PR and NMQ data is less than 1 h, 2) the overlapping area of TRMM PR and NMQ data is larger than 5000 km^2 , and 3) the maximum rainfall rate measured by ground radar is greater than 10 mm h^{-1} to select heavy rain events. These five overpasses, hereinafter referred to as events, have been chosen from five different winter days in 2009 and 2010, since Arizona's climate exhibits precipitation peak during the winter and the bright band is typically low during the cold season. The event descriptions and times are listed in Table 1.

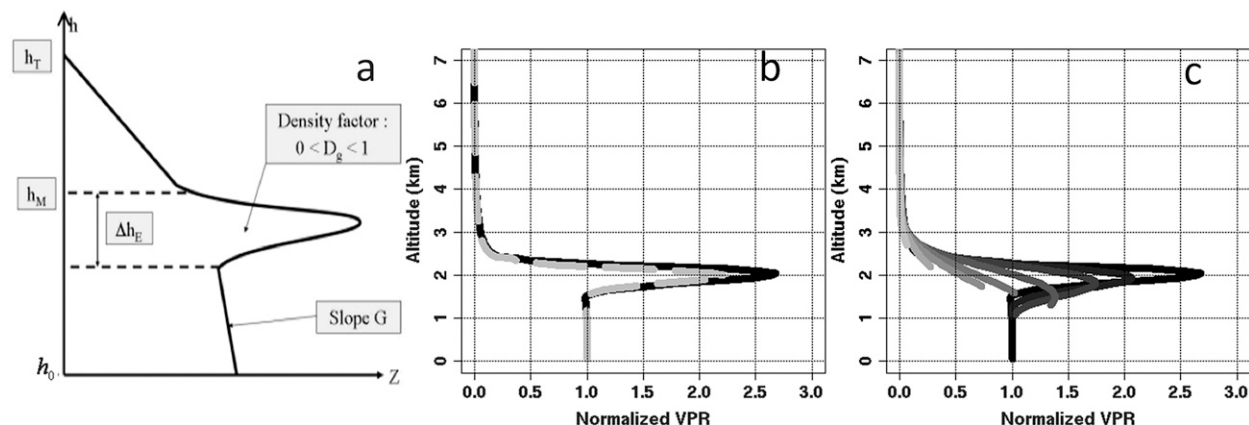


FIG. 2. Steps for incorporating TRMM PR measurements into NMO-QPE (VPR-IE method), using the representative example of the VPR on 8 Dec 2009: (a) fit a physically based VPR model (five parameters) on the Ku-band TRMM PR reflectivity profiles, (b) convert the Ku-band VPR (dotted gray line) into S-band VPR (solid black line), and (c) convolve the S-band VPR with the sampling properties of WSR-88D ground radars. In (c), apparent VPRs are simulated from the S-band VPR from (b) at various distances (from 20 to 240 km with an interval of 20 km) using the beam characteristics of WSR-88D radars.

3. Methodology

a. Overview

The VPR-IE methodology to correct the ground radar-based QPE for VPR sampled from space is summarized in Fig. 2. Note that we follow the formalism from Andrieu and Creutin (1995) and Vignal et al. (1999) and use a normalized VPR (i.e., ratios of reflectivities at different heights versus the reflectivity at a reference height). In doing so, it becomes implicitly assumed that the reflectivity factor $Z(x, h)$ at location x and altitude h can be expressed as the product of its value at the reference level (h_0 , supposed to be 1 km MSL) and the normalized VPR value at the given altitude [see Eq. (1) in Kirstetter et al. 2010]. The VPR for a given precipitation type (e.g., stratiform) is assumed to be homogeneous over the domain of estimation (i.e., over the study area for a given TRMM overpass). Although the TRMM PR

can accurately resolve the vertical reflectivity variations (owing to its sampling geometry and vertical resolution), its measurements cannot match WSR-88D radar measurements because of the frequency difference. For instance, the reflectivity of the brightband peak is generally higher at S band than at Ku band because of the different backscattering cross section.

To use the information from TRMM PR data for ground-radar correction, we have to deal with the frequency difference between the TRMM PR and WSR-88D radars because the VPR shape depends on the wavelength. For instance, the reflectivity of the brightband peak is higher at S band than at Ku band. We therefore need to convert the satellite-based Ku-band VPR to S-band VPR for ground-based radars before correction. This conversion requires using the particle size distribution (PSD), state, and composition of hydrometeors.

TABLE 1. Summary of the events.

Event no.	Events/case study (orbit no.)	Description	TRMM time (UTC)	Q2 time (UTC)	No. of radar-gauge pairs	Freezing-level height (km) (from PR 2A25)
1	8 Feb 2009 (64005)	Moderate stratiform precipitation	1147:03–1148:08	1100–1200	18	2.39
2	8 Dec 2009 (68721)	Heavy precipitation with widespread stratiform; snow in north AZ	0134:52–0135:55	0100–0200	147	2.74
3	22 Jan 2010 (69423)	Heavy precipitation with widespread stratiform	0234:30–0235:32	0200–0300	262	2.50
4	28 Feb 2010 (70003)	Moderate stratiform precipitation; weak convection likely	0740:20–0741:31	0700–0800	238	2.47
5	7 Mar 2010 (70110)	Moderate stratiform precipitation with scattered cells;	0425:48–0426:57	0400–0500	60	2.43

We first identify the vertical distribution of hydrometeors and PSD from the TRMM PR measurements and fit the Ku-band VPR with a physically based model (Fig. 2). This model is then used to simulate the corresponding S-band VPR (Fig. 2b). Finally, this simulated VPR is convolved with ground radar sampling properties to compute apparent ground radar VPRs used for surface QPE computation (Fig. 2c). The volume coverage pattern (VCP) of the current WSR ground radar used for the stratiform events is VCP21. The projection of ground radar-measured reflectivity onto the ground level using the S-band VPR applies a three-dimensional radar beam propagation model by assuming the beam refraction of standard atmospheric conditions and accounting for the earth curvature effect as described by Pellarin et al. (2002), Delrieu et al. (2009), and Kirstetter et al. (2010). The radar beam propagation may change because of the effects of isothermal layer or large temperature inversions, which are not considered here.

b. Physically based VPR model

This section describes a VPR identification method based on a VPR model with several physically based parameters. The VPR model proposed by Kirstetter et al. (2012) and Kirstetter et al. (2013) and derived from Boudevillain and Andrieu (2003) aims at representing the vertical evolution of the equivalent radar reflectivity factor:

$$Z_e(h) = \frac{\lambda^4}{\pi^5 |K_w|^2} \int_0^\infty \sigma[D, \lambda, m(h)] N(D, h) dD, \quad (1)$$

where h is the altitude and σ is the backscattering cross section of a hydrometeor that depends on the equivalent diameter D and the complex refractive index $m(h)$; the refractive index depends on the phase of the hydrometeors and on the radar wavelength λ . The quantity $N(D, h)$ is the number of particles with diameters between D and $D + dD$ per unit diameter range and per unit air volume at altitude h ; $|K_w|^2$ is a constant depending on the refractive index for liquid water m_w . Equation (1) indicates that the equivalent radar reflectivity factor profile depends on 1) the phase of the hydrometeors, which drives their dielectric properties and scattering cross sections through a given scattering model (T matrix, Mie, Rayleigh); 2) PSD, and 3) the radar wavelength. The Z_e value can be appropriated by the sixth moment of PSD if Rayleigh scattering prevails. In practice, Mie scattering may prevail for Ku-band TRMM PR observations because the particle sizes are normally comparable to the wavelength. In such a case, the T-matrix method is applied to compute the Z_e value based on the Mie scattering theory.

The atmospheric column is divided into three vertical layers. The upper layer contains particles of frozen water with air inclusions. In the lowest layer, the precipitation particles are raindrops. The intermediate layer is the melting layer in which particles are composed of a mixture of ice, air and liquid water. These three layers are defined by their altitude boundaries. The top of the precipitating cloud, provided by the radar echo top, is denoted as h_T . The interface between solid and melting layers (the 0°C level for stratiform precipitation) is denoted as h_M , and Δh_E is the melting layer's vertical extension. A reference level close to the ground denoted as h_0 is considered the bottom of the liquid layer. The temperature is assumed to decrease with altitude at the moist adiabatic lapse rate. The scaling formalism initially proposed by Sempere-Torres et al. (1994) is used to describe the relationship between the PSD (assumed as gamma) and the equivalent radar reflectivity factor in the liquid phase and to infer the PSD in the other layers.

The liquid layer is defined between the reference level h_0 and the bottom of the melting layer ($h_M - \Delta h_E$), where hydrometeors are liquid drops. Vertical variations of the equivalent radar reflectivity factor are assumed linear from Z_0 at h_0 to Z_m at $h_M - \Delta h_E$, with a slope G_l . In the solid layer, the hydrometeors are heterogeneous and described by a matrix of ice with inclusions of air. The "matrix inclusion" scheme (Klaassen 1988) is used to retrieve the refractive index of hydrometeors and calculate their dielectric properties. The composition of a solid particle is parameterized using a density factor D_g , varying between 0 (light snow) to 1 (hail) to cover the entire range of mass density of hydrometeors:

$$\rho(h) = \rho_{\min}^{1-D_g} \rho_{\max}^{D_g} \quad \text{with} \quad \rho_{\min} = 5 \quad \text{and} \quad \rho_{\max} = 900 \text{ kg m}^{-3}. \quad (2)$$

The density factor drives the composition of the particles through the ice volume fraction of the total particle volume (Boudevillain and Andrieu 2003; Kirstetter et al. 2012):

$$f_{\text{mat}} = (\rho_{\min}/\rho_{\max})^{1-D_g} \quad \text{and} \quad f_{\text{inc}} = 1 - f_{\text{mat}}, \quad (3)$$

where f_{mat} and f_{inc} are the matrix fraction and the inclusion fraction, respectively. The density factor D_g is part of the calculation of the complex refractive index m through the composition of particles and drives within the dielectric properties of the particles. It is supposed to remain constant in the solid phase and the melting layer. The form of the VPR in the solid layer therefore depends on the PSD defined at the top of the liquid layer

and on D_g . The melting layer is a transitional zone in which the backscattering properties of precipitation particles change rapidly. The possible enhancement of the measured reflectivity by the radar, the bright band, occurs in this zone. The present study uses the simple and convenient scheme proposed by Hardaker et al. (1995), which reproduced the high gradients of reflectivity with a reduced number of variables representative of the PSD, composition, and dielectric properties in this zone. Assuming the PSD to be constant between solid particles and liquid raindrops ensures the continuity of the PSD at the solid/melting and melting/liquid transitions. Particles are composed of a mixture of liquid and solid water with inclusions of air. They are characterized by the melted mass fraction f_m increasing from 0 at the level h_M to 1 at the level $h_M - \Delta h_E$. A two-step processing of the Klaassen (1988) concept and the “matrix inclusion” scheme are applied. By driving the density and the dielectric properties of the particles, D_g controls the enhancement of the bright band. Values of D_g of about 0.8 simulate light iced particles. These particles are more characteristic of stratiform precipitation, and the model simulates an enhanced bright band. Values of D_g of about 1.0 simulate denser particles more often met in convective precipitation. This simple melting layer model could be refined following the results of the series of papers devoted to the brightband description (Szyrmer and Zawadzki 1999).

To summarize, the vertical variations of the equivalent reflectivity factor according to altitude can be represented using a model for the vertical variations of hydrometeors and PSD. These vertical variations of the equivalent reflectivity factor can finally be written $Z_e(h, \varphi)$, while $\varphi = (G_l, h_T, h_M, \Delta h_E, D_g)$ is the vector grouping the five parameters of the VPR model. Note that this set of parameters is relative to the microphysics only and does not depend on the radar wavelength. The VPR, defined as the equivalent reflectivity factor Z_e with altitude, normalized by its value at the reference level Z_0 is expressed as $Z(h, \varphi) = Z_e(h, \varphi)/Z_0$.

c. Enhancement of VPR

For a given event, an optimization procedure adjusts the VPR model to each individual reflectivity profile from the 2A25 product. It uses a quadratic cost function that is minimized with respect to the parameterized profiles of reflectivity using a Gauss–Newton method (Kirstetter et al. 2010). During the optimization procedure, Ku-band VPRs are simulated using the model to match with the TRMM PR measurements. Figure 3 shows the histograms of parameters resulting from the fitting on TRMM PR reflectivity profiles for the case of 8 December 2009. The histograms of the parameters are

typically unimodal, so that a representative VPR may be extracted for the whole stratiform region. The top of the precipitation presents more uncertainties than the other parameters; it may be due to real variations of the vertical extension of the rain field in the region linked to significant elevation differences as well as different PR beam filling conditions and relatively poor sensitivity of the radar (17 dBZ). The most probable values for the density parameter D_g are around 0.85. The retrieved 0°C-level height is for most cases within the range 2400–2600 m altitude, in accordance with the mean value extracted from the 2A25 product (see Table 1). The histogram of the melting layer thickness is highly peaked around 850 m, which is larger than that from long-term brightband observation studies (Fabry and Zawadzki 1995) but is similar to the result of Kitchen et al. (1994) (700 m). Considering the PR vertical resolution and the effect of the radar beam at off-nadir angle, the melting layer thickness of 850 m is considered appropriate for our VPR-IE scheme. Finally, the histogram of the slope of the profile in liquid phase is peaked around 0. More research is needed to investigate the variability of these parameters and the corresponding vertical variations of hydrometeor and PSD.

Our goal is to identify a representative VPR for the whole stratiform region sampled conjointly by ground radar and the PR. The characteristics of this VPR differ from those of the “true” VPR sampled quasi-instantaneously at the PR pixel level because it is representative of a much larger domain. Kirstetter et al. (2010) addressed specifically the issue of VPR homogeneity by performing the VPR identification over areas of homogeneous rain types and consistent microphysical processes. Figure 3 shows that while increasing the representativeness of the VPRs by focusing on the stratiform region (rain type information is from TRMM 2A23 product), the parameters retrieved from the individual 2A25 profiles present variability, which could be caused by microphysics variability inside the stratiform region, noise in the sampled radar reflectivity profiles, and/or simplifications of the physically based VPR model and other factors. A representative VPR for the whole stratiform region may be characterized by a unique set of parameters, $\varphi = (G_l, h_T, h_M, \Delta h_E, D_g)$. We consider the median of each parameter distribution to identify φ . The corresponding VPRs at Ku band and S band for the representative case of 8 December 2009 are shown in Fig. 2b.

We summarize the VPR-IE procedure below:

- A physically based VPR model serves to retrieve the vertical hydrometeor and PSD profiles from the TRMM PR measurements by focusing on the stratiform region.

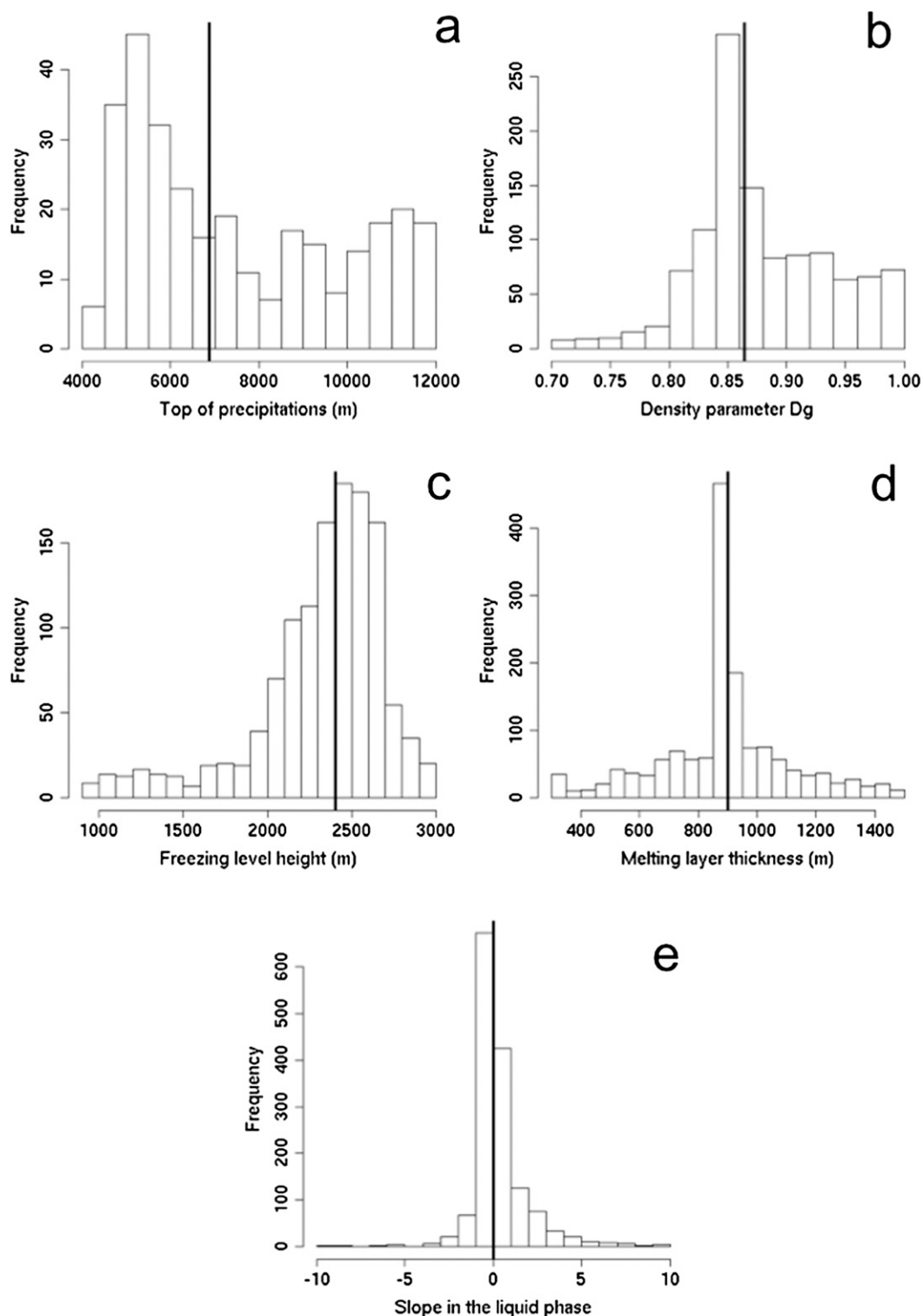


FIG. 3. Histograms of the five parameters of the physically based VPR model fit on TRMM PR reflectivity profiles passing over Arizona at 0135 UTC 8 Dec 2009: (a) the top of precipitation h_T , (b) the density parameter D_g , (c) the 0°C level height h_M , (d) the melting layer thickness Δh_E , and (e) the slope of the profile in liquid phase G_l . The black vertical line in each figure indicates the median value for each parameter.

- This model is used to simulate the corresponding S-band VPR, because the model parameters do not depend on the radar wavelength.
- This representative VPR is convolved with ground radar sampling properties to compute the apparent VPRs.
- The correction is applied to the reflectivity at the corresponding ranges where the apparent VPRs are computed.
- The reflectivity field is converted into rainfall rate using Z - R relations: $Z = 200R^{1.6}$ for stratiform rain and $Z = 300R^{1.4}$ for convective rain. The rainfall rates are then accumulated to hourly rainfall amounts and compared to rain gauge observations.

We assess the approach in the next section by comparing rainfall estimates from the VPR-IE method with respect to the conventional NMQ products and two additional correction methods.

4. Methods for comparison

In this study, we implemented two QPE improvement methods using the TRMM PR as the basis for correction. The two methods are referred to as the rainfall rate calibration method and the rings-based range adjustment method proposed by Gabella et al. (2006), both of which are statistically based correction methods with a lower computational expense compared to the proposed VPR-IE approach. The rainfall rate calibration method is a straightforward calibration, which corrects the ground radar QPE results directly using TRMM PR surface rainfall rate estimates. First, PR surface rainfall rates, which are recorded as a function of latitude and longitude, are remapped onto the NMQ grid having 1-km resolution. We use the PR-interpolated rain field as the basis to calculate the bias of rainfall rate estimation in ground radar-based NMQ. The calculation of bias has been done only for the grid cells having the same precipitation type (e.g., stratiform). After determining the estimation bias, we then calibrate all the NMQ QPE grid cells for a specific precipitation type (Vila et al. 2009).

Gabella et al. (2006) proposed a range adjustment of the ground radar QPE based on the TRMM PR in Israel. The analysis is based on the average of linear radar reflectivity in circular rings around the ground radar site $\langle Z \rangle_{2\pi}$, which is a function of the range from the ground radar site. Factor $F = (\langle \text{GR} \rangle_{2\pi}) / (\langle \text{PR} \rangle_{2\pi})$ is statistically explained using a weighted regression between $\log(F)$ and $\log(\text{Dist})$, where Dist is the distance between a given gauge and the ground radar site. The equation is [Eq. (1) from Gabella et al. 2006]:

$$\begin{aligned} 10 \times \log_{10}(\langle \text{GR} \rangle_{2\pi} / \langle \text{PR} \rangle_{2\pi}) &= F_{\text{dB}} \\ &= a_0 + a_D \log_{10}(\text{Dist} / \text{Dist}_g), \end{aligned} \quad (4)$$

where $\langle \text{GR} \rangle_{2\pi}$ and $\langle \text{PR} \rangle_{2\pi}$ are the average reflectivity in the same 10-km-wide circle ring, averaged in azimuth for both the ground radar and the PR. While $\langle \text{PR} \rangle_{2\pi}$ does not correlate with distance from the ground-based radar site, $\langle \text{GR} \rangle_{2\pi}$ tends to decrease with distance. Dist_g is the reference value of Dist, which is close to the average radar-gauge distance. The a_0 and a_D are two parameters used to modify the calibration of the ground radar measurements. By using all the overpasses collected in Gabella et al. (2006), the resulting parameters are shown as follows:

$$\begin{aligned} 10 \times \log_{10}(\langle \text{GR} \rangle_{2\pi} / \langle \text{PR} \rangle_{2\pi}) \\ = F_{\text{dB}} = -4.1 - 10.1 \times \log_{10}(\text{Dist} / 40). \end{aligned} \quad (5)$$

We have used Eq. (5) for correcting the ground radar observation in this study. More details of this method can be found in Gabella et al. (2006).

5. Case study results

Hourly rain gauges from the Hydrometeorological Automated Data System (HADS; <http://www.nws.noaa.gov/oh/hads/>) and the Maricopa County mesonet have been used to evaluate the three different QPE methods by blending the PR with ground radar observations for five events (summarized in Table 1). It is worth noting that ground radars used for this study have different elevations. As shown in Fig. 1, the elevations of KICX, KFSX, KEMX, KESX, KIWA, and KYUX radars are 3231, 2261, 1586, 1509, 421, and 53 m MSL, respectively. Given a storm system in the cold season, the radar beam could overshoot cloud tops or intercept the melting layer at far ranges, especially for KICX, KFSX, KEMX, and KESX radars. According to the locations of rain gauges shown in Fig. 1, the QPE based on KFSX radar is most likely affected by the melting layer. Figure 4 shows a comparison of hourly rainfall from remote sensing data and rain gauge measurements, with the three panels corresponding to the three different methods of blending PR with ground radar observations. Data shown in this analysis are from all five events combined. The black dots in the figure indicate the ground radar QPE without any adjustment from PR. Most points seem to be plagued by either underestimation or overestimation. Considering the height of the 0°C level in the cold season and the position of the radar beam in this complex terrain, overestimation is likely due to sampling in the bright band, while underestimation is likely attributed to

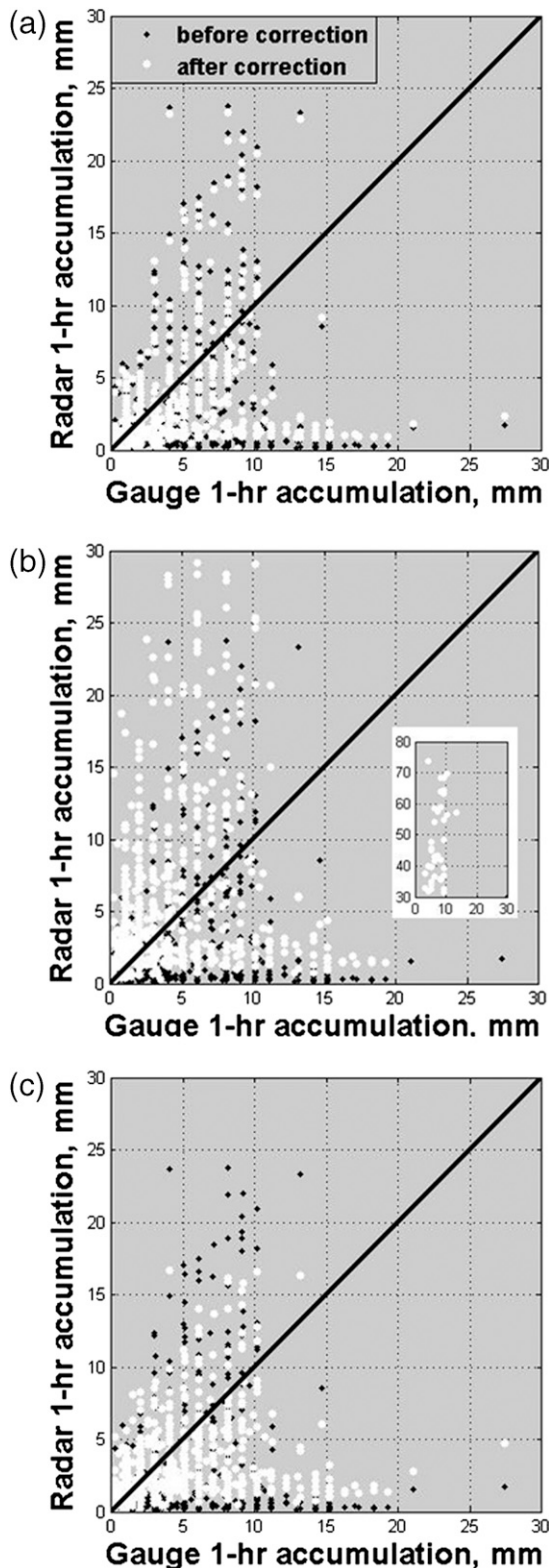


FIG. 4. Scatterplots of 1-h radar precipitation estimates before (black diamonds) and after (white circles) the corrections for all five events combined using the (a) rainfall rate calibration method, (b) rings-based range adjustment with inset extending values to 80 mm, and (c) VPR-IE method. The black line is the 1:1 line.

sampling frozen hydrometeors above the 0°C level. The simple rainfall rate calibration method (Fig. 4a) shows some improvements over the QPE, although not significant. The correction using the rings-based range adjustment method (Fig. 4b) generally reduced the underestimation but resulted in erroneous overestimation. This was due to the monotonic linear model used in the correction scheme, where overestimation errors associated with the bright band and underestimation errors associated with radar sampling in the ice region could not be simultaneously accounted for. The underestimation errors might have dominated the linear regression model, and, as a result, the overestimation error did not get corrected but was instead exaggerated. Figure 4c shows the QPE result obtained with the VPR-IE method introduced in section 3. This method mitigates both overestimation and underestimation of rainfall, showing a much better agreement with gauge observations than the other two methods.

Figure 5 provides hourly rainfall maps with and without applying the VPR-IE method (results using the other two methods are not shown) for each case study. For example, Fig. 5c shows a widespread stratiform precipitation on 8 December 2009, for which the 0°C level was about 1800, 1800, 2100, 2500, 2600, and 2800 m for the KICX, KESX, KFSX, KIWA, KYUX, and KEMX radars, respectively. Note that these 0°C level heights are consistent with the histogram of the 0°C levels from the VPR model approach (see Fig. 3c). For most rainy areas shown in this figure, the radar beam has overshot the melting layer. The measurements within the ice region led to underestimation of rainfall on the surface from the original NMQ QPE product at lower elevations (Fig. 5c). After the VPR-IE method was applied (Fig. 5d), the underestimation was mitigated, especially in areas 100 km east of KESX and 50 km southeast of KFSX. Another example is 28 February 2010, for which the 0°C level was 2400–2600 m within the area from 33.5° to 34°N in latitude and from -113° to -112°W in longitude. KFSX's radar beam intercepted the melting layer in this area, causing an overestimation of rainfall in the original NMQ QPE as shown in Fig. 5g. The VPR-IE product (Fig. 5h) reduced this apparent overestimation. On the other hand, similar to the analysis in Figs. 5c and 5d, at the further range (e.g., >100 km) where the radar beam has overshot the melting layer and samples in the ice region, the VPR-IE method has increased the estimate of rainfall, which was previously underestimated.

From the five events shown in Fig. 5, three statistical indices have been calculated to evaluate the performance of the three correction methods. Relative bias (RB; in percent) is used to assess the systematic bias of radar estimations. The mean absolute error (MAE) measures the average magnitude of the error. The root-mean-squared

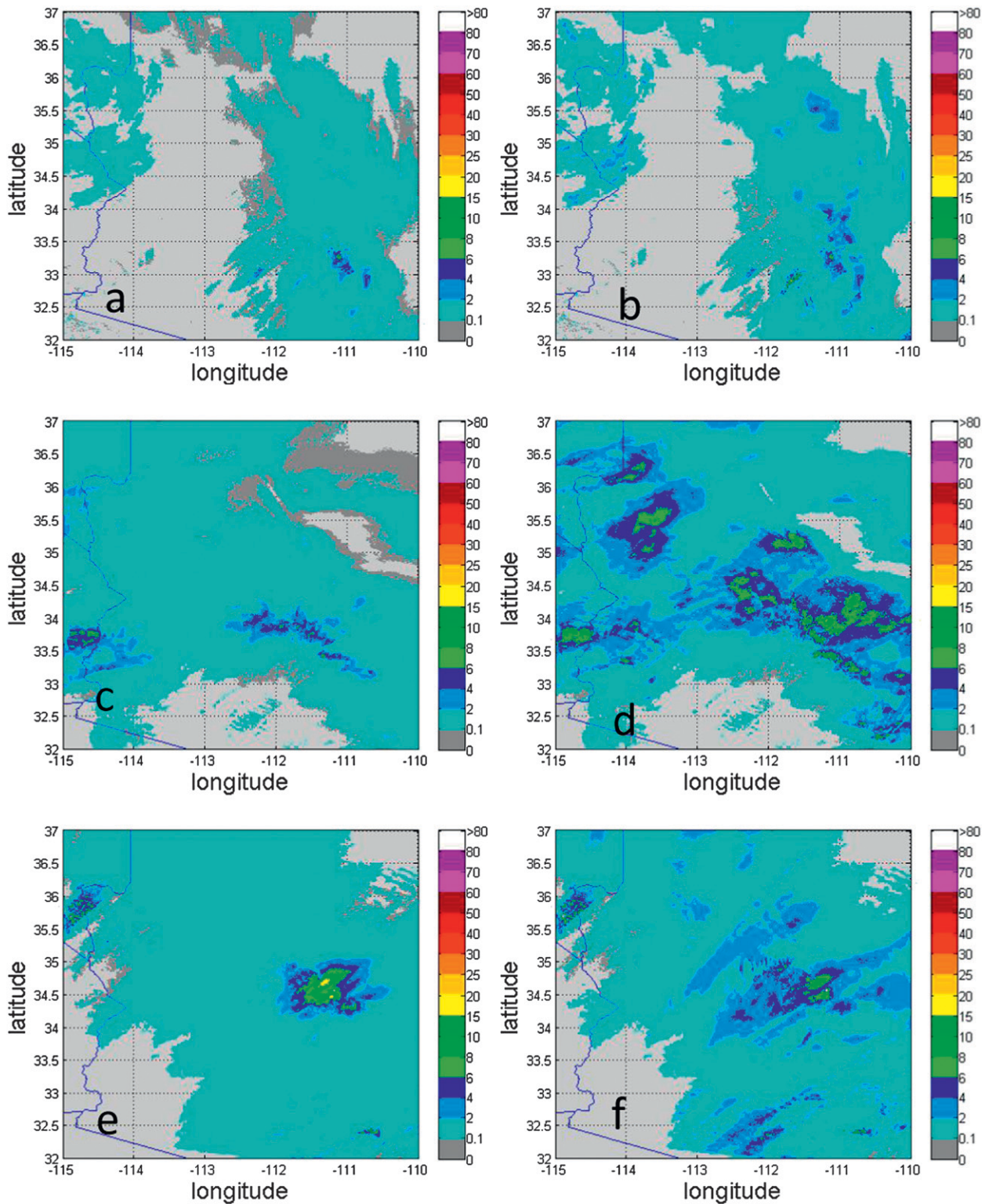


FIG. 5. Sequential 1-h radar precipitation accumulation (mm) estimates (left) before and (right) after adjustment using the VPR-IE method: (a),(b) 8 Feb 2009; (c),(d) 8 Dec 2009; (e),(f) 22 Jan 2010; (g),(h) 28 Feb 2010; and (i),(j) 7 Mar 2010.

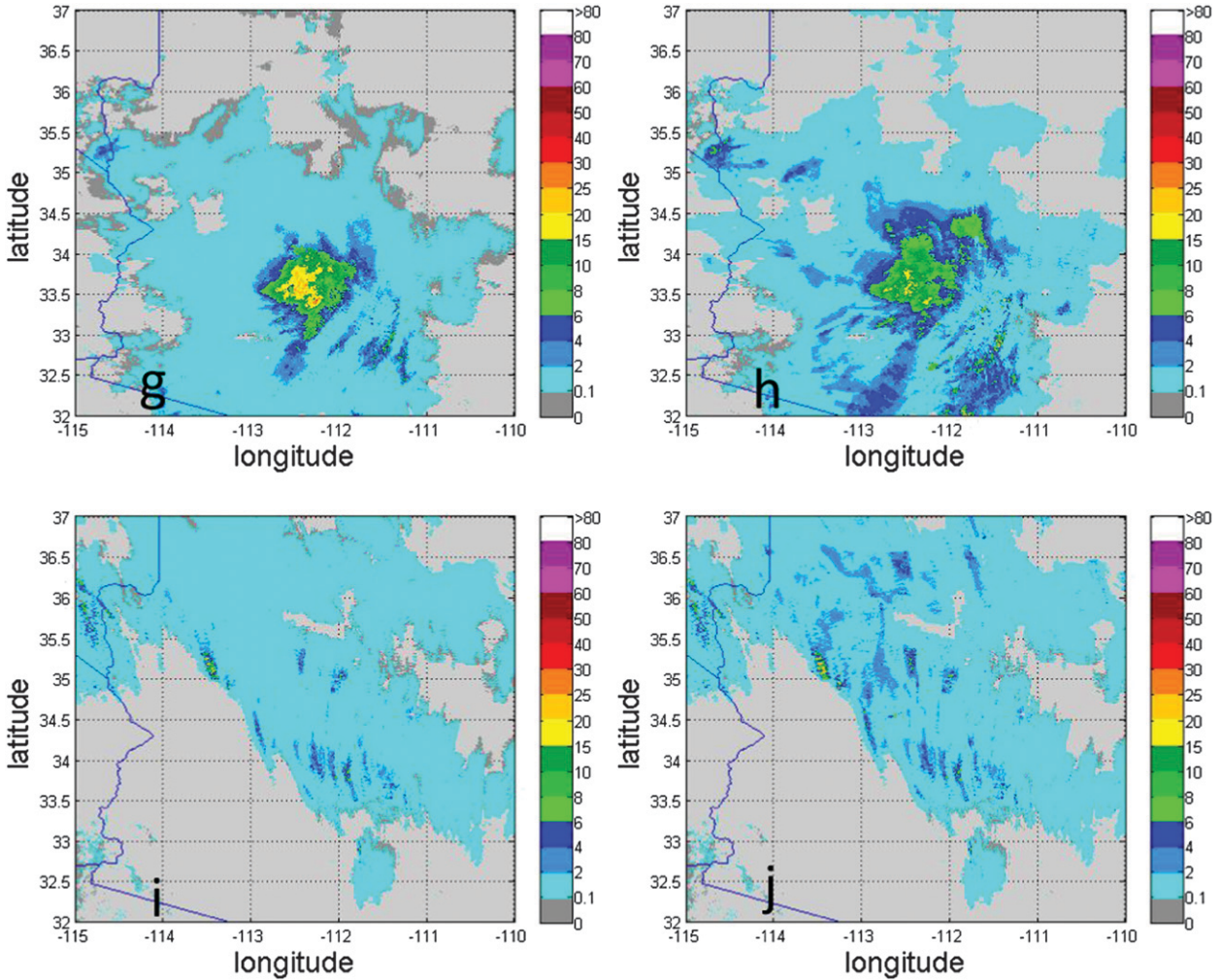


FIG. 5. (Continued)

error (RMSE) is another way to quantify the average error magnitude, giving greater weights to larger errors. MAE and RMSE are in units of millimeters for the comparison of estimated rainfall amounts:

$$RB = \frac{\sum_{i=1}^N R(i) - \sum_{i=1}^N G(i)}{\sum_{i=1}^N G(i)} \times 100\%, \quad (6)$$

$$MAE = \frac{\sum_{i=1}^N |R(i) - G(i)|}{N}, \quad (7)$$

$$RMSE = \sqrt{\frac{\sum_{i=1}^N |R(i) - G(i)|^2}{N}}. \quad (8)$$

Here, $R(i)$ and $G(i)$ represent the i th matching pair of rainfall amounts estimated with radar reflectivity and observed by rain gauges, respectively, and N represents the total number of data pairs for radar-based and rain gauge data matching. The following two criteria have been used for matching data: 1) the gauge location is within one of the $0.01^\circ \times 0.01^\circ$ radar grid cells used in NMQ/Q2 and 2) both $R(i)$ and $G(i)$ are greater than zero.

The statistics have been computed with hourly rainfall estimates and are shown in Table 2 for all five events. The Q2 columns denote the results calculated from the original ground radar-only product of NMQ/Q2. The best statistical performances among the three methods are highlighted in bold. Generally speaking, the third method (i.e., VPR-IE method) has the best overall performance compared to the other three approaches. The rings-based range adjustment (i.e., the second method)

TABLE 2. Statistical results of the three TRMM PR-based correction approaches: I is the rainfall rate calibration method, II is the rings-based range adjustment method, and III is the VPR-IE method. The method with the best performance according to the statistic is denoted in boldface.

<i>E</i>	RB (%)				MAE				RMSE			
	Q2	I	II	III	Q2	I	II	III	Q2	I	II	III
1	-69.08	-80.40	-26.27	-50.40	0.63	0.75	0.75	0.48	1.18	1.30	1.19	0.94
2	-39.52	-28.19	71.05	-12.58	1.36	1.31	2.51	1.00	2.39	2.30	4.10	1.55
3	-85.90	-75.19	-58.04	-68.60	4.27	3.80	3.43	3.50	6.25	5.82	5.36	5.45
4	29.55	18.15	242.99	13.87	2.44	2.46	10.23	1.75	3.98	3.85	17.17	2.54
5	-16.93	-36.05	154.85	-5.09	0.97	0.98	3.09	0.98	1.89	1.91	4.44	1.81
All	-38.23	-36.02	69.17	-21.09	2.64	2.53	5.30	2.15	4.50	4.29	10.47	3.93

has the least improvements. This result is likely due to the monotonic linear empirical relation for range adjustment [Eq. (5)], which is insufficient to simultaneously correct for both overestimation in the melting layer and underestimation with increasing range when sampling in the ice region. However, it is interesting to see this method performs the best for event #3 on 22 January 2010, which was a widespread stratiform event with a 0°C level from 2000 to 3000 m, gradually increasing in altitude from northwest to southeast within the analysis region. The KIWA radar was not working during this case, and ground radar observations mainly came from KICX, KESX, KFSX, and KEMX radars. As a result, all ground radar observations were above the melting layer and were affected by beam overshooting alone rather than underestimation combined with overestimation by sampling in the bright band (Fig. 5e). Significant underestimations of surface rainfall are indicated in Table 2 (underestimated by 58.04%–85.9%) for all QPE approaches. The MAE and RMSE values are high as well. The VPR-IE does not show improvements over the rings-based range adjustment in this particular case where the variation of the 0°C level from 2000 to 3000 m. This result implies that one representative VPR might not be sufficient to account for the variability of the vertical structure of precipitation in this region, warranting additional research.

Events #2 and #4 on 8 December 2009 and 28 February 2010 demonstrate superior performance of the VPR-IE correction method. Ground radar beam overshooting was a major issue in the former event while the interception of the melting layer was more evident in the latter event. Table 2 shows effective mitigation of both underestimation and overestimation, with the RB changing from -39.5% to -12.58% and from 29.55% to 13.87%, respectively. The estimation errors (MAE and RMSE) are also reduced greatly. The simple rainfall rate calibration method I improved the bias over the uncorrected, radar-only method in both these cases, while the rings-based method II increased the bias up to 243% in event #4.

Systematic error of ground-based radar rainfall estimation, related to the VPR features combined with the geometric effects of the radar beam, creates the often-noted radar range dependence (Bellon et al. 2005; Krajewski et al. 2011). Figure 6 shows the range-dependent multiplicative bias [(radar - rain gauge)/rain gauge ratios] as a function of distance from the radar for events #2 and #3. Considering the relative position of the rain gauge network to the radar sites, the observations evaluated in this figure mainly come from the KIWA radar for distances within 100 km of it and the KFSX radar. We recall the 8 December 2009 event #2 corresponds to a 0°C-level height of 2500 m, while the KIWA radar altitude is 421 m. For the uncorrected QPE, the contamination of the radar beam by the bright band leads to bias values exceeding 0 around a range of 70 km, and the overshooting of the radar beam in the ice phase at distances greater than 100 km causes the far range underestimation (Andrieu and Creutin 1995). The VPR-IE using the TRMM PR information mitigates significantly the range-dependent error. We recall that for the 22 January 2010 event #3 the KIWA radar data were not available, so the range-dependent error is mainly for observations from the KFSX radar. Its altitude is 2261 m while the 0°C-level height was around 2600 m, causing contamination of the radar beam by the bright band at close ranges. The unadjusted radar QPE consistently shows an overestimation relative to rain gauges up to 60 km, followed by an underestimation likely due to the ice phase sampling. The VPR-IE using the TRMM PR information mitigates this range-dependent error.

6. Summary and conclusions

In this study, we have demonstrated the effective integration of the Ku-band TRMM PR products (radar reflectivity, precipitation type, and quantity at 4-km horizontal and 250-m vertical resolutions) into the NMQ system to improve the S-band ground-based radar rainfall estimation. Our major interest focuses on mountainous

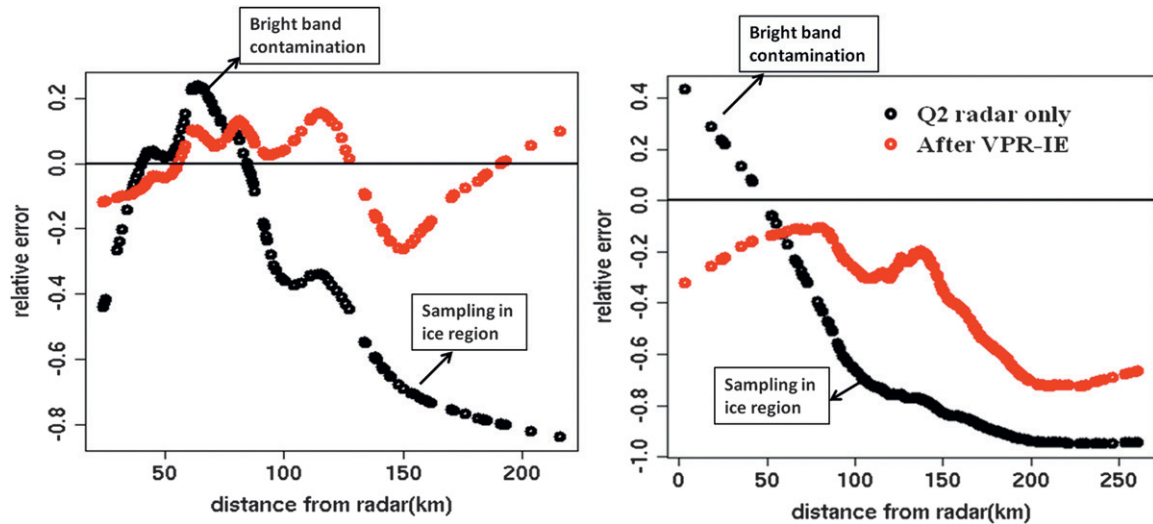


FIG. 6. QPE error [(radar – rain gauge)/rain gauge] in terms of range for the (left) 8 Dec 2009 case and (right) 22 Jan 2010 case.

regions where beam blockages, overshooting, and intercepting the melting layer remain the major problems for ground radar-based QPE. This study proposes a VPR-IE method to improve the surface rainfall estimate in the Mountain States region by synergistically integrating observations from spaceborne TRMM PR into NEXRAD-based radar products. With the physically based VPR model, the TRMM 3D reflectivity profile (Ku band) is used to derive a representative VPR at S band within a specific region (e.g., a region of stratiform precipitation). Surface rainfall estimates, which were previously hampered by sampling within or above the melting layer, can be greatly improved through the incorporation of the TRMM-observed VPR data. Recently, an empirical conversion approach has also been introduced to convert TRMM PR's Ku-band VPR to S-band VPR (Cao et al. 2013b). The empirical approach avoids the nonlinear fitting to the physically based VPR model and has computational efficiency for VPR-IE to be implemented in real time.

The VPR-IE method has been evaluated with several stratiform precipitation events in Arizona. Two other statistically based correction methods, TRMM-based rainfall calibration and the rings-based range adjustment, have also been compared with the physically based VPR method. The statistical analysis shows that the VPR-IE method has the best overall performance and provides much more accurate surface rainfall estimates than the original radar QPE in the current NMQ system for the study region. Although the evaluation is based on a limited number of precipitation events, the potential of the VPR-IE method has been demonstrated to utilize spaceborne radar observations in improving

surface radar QPE, especially in mountainous regions, was demonstrated. The proposed VPR-IE method can be further improved to better account for the spatial variability of precipitation and the temporal resolution difference between TRMM and NMQ data. Also, the U.S. National Weather Radar Network is being upgraded to include polarimetric capabilities, which will provide more microphysics information for QPE study. Cao et al. (2013a) characterized the seasonal, spatial, intensity-related, and type-related variability for the PR's VPR, as well as the heights of storm, freezing level, and bright band. Using the PR-derived climatological VPR information can solve the intermittent issue of PR data and makes the VPR-IE method more feasible. But there are still many issues, such as the conversion from Ku-band to S-band reflectivity and the spatiotemporal representativeness, which must be addressed using climatological VPR. These issues will be addressed and reported on in future studies. Our ultimate goal is to develop an automated VPR-IE scheme by synergistically incorporating TRMM PR and to-be-launched Global Precipitation Measurement (GPM) Dual-Frequency PR into the NMQ system for enhancing ground radar QPE products, particularly in the mountainous regions of the United States.

Acknowledgments. This work was financially supported by the NOAA Multi-Function Phased-Array Radar Project administrated by the Advanced Radar Research Center at the University of Oklahoma. The authors gratefully acknowledge the NSSL/OU NMQ research group and the NASA GPM Ground Validation and SPoRT Programs.

REFERENCES

- Andrieu, H., and J. D. Creutin, 1995: Identification of vertical profiles of radar reflectivity for hydrological applications using an inverse method. Part I: Formulation. *J. Appl. Meteor.*, **34**, 225–239.
- Bellon, A., G.-W. Lee, and I. Zawadzki, 2005: Error statistics of VPR corrections in stratiform precipitation. *J. Appl. Meteor.*, **44**, 998–1015.
- Boudevillain, B., and H. Andrieu, 2003: Assessment of vertically integrated liquid (VIL) water content radar measurement. *J. Atmos. Oceanic Technol.*, **20**, 807–819.
- Cao, Q., Y. Hong, J. J. Gourley, Y. Qi, J. Zhang, Y. Wen, and P.-E. Kirstetter, 2013a: Statistical and physical analysis of vertical structure of precipitation in mountainous west region of the United States using 11+ years of spaceborne Observations from TRMM precipitation radar. *J. Appl. Meteor. Climatol.*, **52**, 408–424.
- , —, Y. Qi, Y. Wen, J. Zhang, J. Gourley, and L. Liao, 2013b: Empirical conversion of vertical profile of reflectivity from Ku-band to S-band frequency. *J. Geophys. Res.*, **118**, 1814–1825, doi:10.1002/jgrd.50138.
- Delrieu, G., B. Boudevillain, J. Nicol, B. Chapon, P.-E. Kirstetter, H. Andrieu, and D. Faure, 2009: Bollène 2002 experiment: Radar rainfall estimation in the Cévennes–Vivarais region. *J. Appl. Meteor. Climatol.*, **48**, 1422–1447.
- Fabry, F., and I. Zawadzki, 1995: Long-term radar observations of the melting layer of precipitation and their interpretation. *J. Atmos. Sci.*, **52**, 838–851.
- Gabella, M., J. Joss, G. Perona, and S. Michaelides, 2006: Range adjustment for ground-based radar, derived with the spaceborne TRMM precipitation radar. *IEEE Trans. Geosci. Remote Sens.*, **44**, 126–133.
- Germann, U., and J. Joss, 2002: Mesobeta profiles to extrapolate radar precipitation measurements above the Alps to the ground level. *J. Appl. Meteor.*, **41**, 542–557.
- Hardaker, P. J., A. R. Holt, and C. G. Collier, 1995: A melting-layer model and its use in correcting for the bright band in single-polarization radar echoes. *Quart. J. Roy. Meteor. Soc.*, **121**, 495–525.
- Iguchi, T., T. Kozu, R. Meneghini, J. Awaka, and K. Okamoto, 2000: Rain-profiling algorithm for the TRMM Precipitation Radar. *J. Appl. Meteor.*, **39**, 2038–2052.
- , —, J. Kwiatkowski, R. Meneghini, J. Awaka, and K. Okamoto, 2009: Uncertainties in the rain profiling algorithm for the TRMM precipitation radar. *J. Meteor. Soc. Japan*, **87**, 1–30.
- Joss, J., and R. Lee, 1995: The application of radar-gauge comparisons to operational precipitation profile corrections. *J. Appl. Meteor.*, **34**, 2612–2630.
- Kirstetter, P. E., H. Andrieu, G. Delrieu, and B. Boudevillain, 2010: Identification of vertical profiles of reflectivity for correction of volumetric radar data using rainfall classification. *J. Appl. Meteor. Climatol.*, **49**, 2167–2180.
- , —, B. Boudevillain, and G. Delrieu, 2012: Toward a physically-based identification of vertical profiles of reflectivity from volume scan radar data. *IAHS Publ.*, **351**, 194–200.
- , —, —, and —, 2013: A physically based identification of vertical profiles of reflectivity from volume scan radar data. *J. Appl. Meteor. Climatol.*, in press.
- Kitchen, M., 1997: Towards improved radar estimates of surface precipitation at long range. *Quart. J. Roy. Meteor. Soc.*, **123**, 145–163.
- , R. Brown, and A. G. Davies, 1994: Real-time correction of weather radar data for the effects of bright band, range and orographic growth in widespread precipitation. *Quart. J. Roy. Meteor. Soc.*, **120**, 1231–1254.
- Klaassen, W., 1988: Radar observations and simulation of the melting layer of precipitation. *J. Atmos. Sci.*, **45**, 3741–3752.
- Koistinen, J., 1991: Operational correction of radar rainfall errors due to the vertical reflectivity profile. Preprints, *25th Int. Conf. on Radar Meteorology*, Paris, France, Amer. Meteor. Soc., 91–94.
- Krajewski, W. F., B. Vignal, B.-C. Seo, and G. Villarini, 2011: Statistical model of the range-dependent error in radar-rainfall estimates due to the vertical profile of reflectivity. *J. Hydrol.*, **402**, 306–316.
- Lakshmanan, V., A. Fritz, T. Smith, K. Hondl, and G. J. Stumpf, 2007: An automated technique to quality control radar reflectivity data. *J. Appl. Meteor. Climatol.*, **46**, 288–305.
- Maddox, R., J. Zhang, J. J. Gourley, and K. Howard, 2002: Weather radar coverage over the contiguous United States. *Wea. Forecasting*, **17**, 927–934.
- Matrosov, S. Y., K. A. Clark, and D. E. Kingsmill, 2007: A polarimetric radar approach to identify rain, melting-layer, and snow regions for applying corrections to vertical profiles of reflectivity. *J. Appl. Meteor. Climatol.*, **46**, 154–166.
- Pellarin, T., G. Delrieu, G.-M. Saulnier, H. Andrieu, B. Vignal, and J.-D. Creutin, 2002: Hydrologic visibility of weather radar systems operating in mountainous regions: Case study for the Ardèche catchment (France). *J. Hydrometeorol.*, **3**, 539–555.
- Sellers, W. D., and R. H. Hill, 1974: *Arizona Climate 1931–1972*. University of Arizona Press, 616 pp.
- Sempere-Torres, D., J. M. Porrà, and J.-D. Creutin, 1994: A general formulation for raindrop size distribution. *J. Appl. Meteor.*, **33**, 1494–1502.
- Simpson, J., C. Kummerow, W.-K. Tao, and R. F. Adler, 1996: On the tropical rainfall measuring mission (TRMM). *Meteor. Atmos. Phys.*, **60**, 19–36.
- Smith, J. A., D.-J. Seo, M. L. Baeck, and M. D. Hudlow, 1996: An intercomparison study of NEXRAD precipitation estimates. *Water Resour. Res.*, **32**, 2035–2045.
- Smyth, T. J., and A. J. Illingworth, 1998: Radar estimates of rainfall rates at the ground in bright band and non-bright band events. *Quart. J. Roy. Meteor. Soc.*, **124**, 2417–2434.
- Szyrmer, W., and I. Zawadzki, 1999: Modeling of the melting layer. Part I: Dynamics and microphysics. *J. Atmos. Sci.*, **56**, 3573–3592.
- Tabary, P., 2007: The new French operational radar rainfall product. Part I: Methodology. *Wea. Forecasting*, **22**, 393–408.
- Vasiloff, S., and Coauthors, 2007: Improving QPE and very short term QPF: An initiative for a community-wide integrated approach. *Bull. Amer. Meteor. Soc.*, **88**, 1899–1911.
- Vignal, B., and W. F. Krajewski, 2001: Large-sample evaluation of two methods to correct range-dependent error for WSR-88D rainfall estimates. *J. Hydrometeorol.*, **2**, 490–504.
- , H. Andrieu, and J. D. Creutin, 1999: Identification of vertical profiles of reflectivity from volume-scan radar data. *J. Appl. Meteor.*, **38**, 1214–1228.
- , G. Galli, J. Joss, and U. Germann, 2000: Three methods to determine profiles of reflectivity from volumetric radar data to correct precipitation estimates. *J. Appl. Meteor.*, **39**, 1715–1726.
- Vila, D. A., L. G. G. De Goncalves, D. L. Toll, and J. R. Rozante, 2009: Statistical evaluation of combined daily gauge observations

- and rainfall satellite estimates over continental South America. *J. Hydrometeor.*, **10**, 533–543.
- Watson, A. I., R. E. Lopez, and R. L. Holle, 1994: Diurnal cloud-to-ground lightning patterns in Arizona during the southwest monsoon. *Mon. Wea. Rev.*, **122**, 1716–1725.
- Wen Y., Y. Hong, G. Zhang, T. J. Schuur, J. J. Gourley, Z. Flamig, K. R. Morris, and Q. Cao, 2011: Cross validation of spaceborne radar and ground polarimetric radar aided by polarimetric echo classification of hydrometeor types. *J. Appl. Meteor. Climatol.*, **50**, 1389–1402.
- Yong, B., L.-L. Ren, Y. Hong, J.-H. Wang, J. J. Gourley, S.-H. Jiang, X. Chen, and W. Wang, 2010: Hydrologic evaluation of Multisatellite Precipitation Analysis standard precipitation products in basins beyond its inclined latitude band: A case study in Laohahe basin, China. *Water Resour. Res.*, **46**, W07542, doi:10.1029/2009WR008965.
- Zhang, J., and Y. Qi, 2010: A real-time algorithm for the correction of brightband effects in radar-derived QPE. *J. Hydrometeor.*, **11**, 1157–1171.
- , K. Howard, and J. J. Gourley, 2005: Constructing three-dimensional multiple-radar reflectivity mosaics: Examples of convective storms and stratiform rain echoes. *J. Atmos. Oceanic Technol.*, **22**, 30–42.
- , and Coauthors, 2011: National Mosaic and Multi-sensor QPE (NMQ) system: Description, results, and future plans. *Bull. Amer. Meteor. Soc.*, **92**, 1321–1338.